ChemBioChem

Chemistry Europe
European Chemical Societies Publishing
ChemBioChem

RESEARCH ARTICLE OPEN ACCESS

Ultraviolet Raman Optical Activity as a Window Into Peptide Backbone Structure

Ondřej Škrna[1] | Josef Kapitán[2] | Laurence D. Barron[3] | Petr Bouř[4]

[1]ETH Zurich, Zurich, Switzerland | [2]Department of Optics, Palacký University Olomouc, Olomouc, Czech Republic | [3]Department of Chemistry, University of Glasgow, Glasgow, UK | [4]Institute of Organic Chemistry and Biochemistry, Academy of Sciences, Prague, Czech Republic

Correspondence: Josef Kapitán (kapitan@optics.upol.cz) | Petr Bouř (bour@uochb.cas.cz)

Received: 23 February 2026 | **Revised:** 13 March 2026 | **Accepted:** 17 March 2026

Keywords: density functional theory | molecular dynamics | optical activity | peptide structure | Raman | resonance

ABSTRACT

The spectroscopy of ultraviolet Raman optical activity (UV ROA) promises an excellent sensitivity to peptide and protein conformation, decoupling the backbone signal from most side chains. Compared to the more usual ROA with visible light, stronger intensity and additional spatial sensitivity are expected because most of the signal comes from the amide chromophore. UV ROA experiments are scarce, and links between spectral shapes and molecular structure are rather unexplored. However, on a dedicated instrument, we could acquire spectra of three peptides and analyze them on the basis of molecular dynamics and density functional theory simulations. Radical differences were observed between the spectra obtained with the 244 and 532 nm excitations, and they could be rationalized by the simulations. Bands connected to the peptide backbone vibrations are enhanced at the shorter wavelength, due to a pre-resonance with the n-π* and π-π* amide transitions. Further computational experiments on the Ala_4 peptide indicate that sensitivity to the secondary structure is enhanced as well, by a combination of geometric and resonance effects. The results thus confirm the potential of UV ROA for analytical chemistry and biochemistry in terms of novel information it brings about molecular geometric and electronic structure.

1 | Introduction

Similarly as ultraviolet Raman spectroscopy [1], ultraviolet Raman optical activity (UV ROA) has been mainly pursued for the signal enhancement it provides if compared to excitations with visible (VIS) or near infrared (NIR) light [2]. The spectra can thus be in principle collected faster, with a smaller amount of sample, or in smaller concentrations. In addition, sample fluorescence can be avoided due to a large wavenumber gap between the Raman and fluorescence signals. Compared to unpolarized Raman scattering, UV ROA is not only sensitive to chirality, but it is also much more responsive to minor differences in molecular structure. Because of the selective enhancement of vibrations related to molecular parts absorbing the excitation light, effective increase in spatial resolution can be achieved as well [3]. The spectroscopy thus provides a welcome extension to methods of vibrational optical activity for studies of protein folding [4], biomolecular aggregation [5], molecular origin of neurodegenerative diseases [6, 7], and other biological problems.

In reality, these advantages come with price, and UV experiments are quite challenging. The UV light quickly damages many samples, corresponding optics is more expensive than for visible light, and so are the lasers and detectors. The signal can be contaminated with electronic circular dichroism combined with polarized Raman scattering (ECD-Raman effect) [8, 9].

There are also some difficult or even unresolved theoretical issues connected to simulation and interpretation of the "resonance" spectra, i.e., where the energy of the excitation laser beam is close to an electronic transition. Sometimes, combination or overtone bands appear in resonance [10, 11], requiring accounting for the anharmonic effects [12]. The usual Born-Oppenheimer [13] and Placzek [14, 15] approximations must be used carefully. For example, a strict separation of the electronic and nuclear

wave functions is not possible [16, 17], and usual analytical computations of frequency-dependent polarizability derivatives needed to model spectral intensities may not be adequate [18]. In the case of single electronic state (SES) limit, the ROA signal can just be proportional to the Raman one, thus significantly reducing information one can get from the spectra [19].

In spite of these problems, given the dynamic development of various ROA experimental modalities and theory, conquering the UV region seems inevitable. First UV ROA spectrometer operating with the 244 nm excitation has already been reported [20]; in the present study we analyze spectra obtained with it. The UV light is a logical extension and broadens the possibilities of the technique, usually focused on excitations with visible wave lengths (such as 488, 514.5 and 532 nm) [21, 22], but expanding to the near infrared (NIR) region as well [23]. In fact, 788 nm can now be used routinely [24], and 1064 nm was suggested [25]. The NIR spectrometers usually provide reduced fluorescence, similarly as for UV ROA; however, their signal to noise ratio is quite low, which makes their use for many application problematic.

Below, we briefly review the theoretical background of UV ROA and explore the performance of the couple-perturbed density functional theory (DFT) computations of the intensities [26, 27]. Model molecules include Ala-Ala zwitterion (alanyl-alanine, dialanine), its cyclic form c-Ala-Ala (cyclodialanine), and Ala_4 tetrapeptide cation: Due to the locality of vibrational spectra [28, 29], they are reasonable models for peptide and protein behavior, while their small size allows for detailed computational modeling. It turns out that the theory is adequate to predict and explain the experimental data, such as the origin of selective enhancement of particular Raman and ROA bands compared to visible excitations. The experimental data also confirm the huge intensity and ROA/Raman ratio (so called circular intensity difference, CID) [30] in UV predicted by the theory. Once the validity of the computational protocol is confirmed on smaller molecules, computations on the tetraalanine peptide allow us to investigate the ability of UV ROA to distinguish standard peptide and protein conformations.

2 | Theoretical Background

The importance of the excitation wavelength for molecular Raman scattering is evident from the principal molecular properties determining Raman and ROA intensities. These are primarily the transition polarizabilities [30, 31]. Neglecting fine vibronic effects [16, 32], we need three of them, electric dipole - electric dipole (α), electric dipole–magnetic dipole (G), and electric dipole–electric quadrupole (A) one, with Cartesian components

$$\alpha_{\alpha\beta} = \frac{2}{\hbar}\sum_{e\neq 0}\frac{\omega_{e0}\langle m|\mu_{0e\alpha}\mu_{e0\beta}|n\rangle}{\omega_{e0}^2-\omega^2} \tag{1}$$

$$G_{\alpha\beta} = -\frac{2\omega}{\hbar}\sum_{e\neq 0}\frac{\langle m|\mu_{0e\alpha}m_{e0\beta}|n\rangle}{\omega_{e0}^2-\omega^2} \tag{2}$$

$$A_{\alpha,\beta\gamma} = \frac{2}{\hbar}\sum_{e\neq 0}\frac{\omega_{e0}\langle m|\mu_{0e\alpha}\Theta_{e0\beta\gamma}|n\rangle}{\omega_{e0}^2-\omega^2} \tag{3}$$

where $\omega_{e0} = \omega_e - \omega_0$ is the difference of angular frequencies of electronic excited (e) and ground (0) states, ω is the excitation frequency, $\hbar$ is the reduced Planck constant, n is the initial (typically ground), m is the final vibrational state, and $\mu_{0e\alpha} = \langle e|\mu_\alpha|0\rangle$ is the α-component of the transition dipole moment between electronic ground excited states (similarly for the magnetic dipole m_β and electric quadrupole $\Theta_{\beta\gamma}$).

These expressions can be easily adapted for resonance when $\omega_{e0} = \omega$ [15]. However, we are interested in a pre-resonance case, in particular in the 244 nm experiment [20], where the excitation energy is still quite far from the lowest-energy amide transition, typically below 220 nm [33]. In this case, we can use the Placzek approximation [14] and an analytical DFT coupled-perturbed approach when the transition polarizabilities are calculated from derivatives [26]. This is implemented, for example, in Gaussian [34] and other quantum-chemical programs. For α and a fundamental ($0 \rightarrow 1$) transition of vibrational normal mode i, within the harmonic approximation,

$$\alpha_{\alpha\beta} \sim \left\langle 1\left|\alpha_{\alpha\beta}^{(e)}\right|0\right\rangle \sim \frac{\partial\alpha_{\alpha\beta}^{(e)}}{\partial Q_i}\sqrt{\frac{\hbar}{2\omega_i}} \tag{4}$$

where $\alpha_{\alpha\beta}^{(e)}$ is the electronic polarizability, Q_i is the normal mode coordinate, and ω_i is the vibrational frequency. Analogous expressions are obtained for G and A.

We model the common back-scattered circular polarization (SCP) modulation, which is in the pre-resonance case equivalent to the incident circular polarization (ICP) one. For an isotropic sample, Raman and ROA intensities are given by [2, 15]

$$I_{Raman} = K\sum_{\alpha=1}^{3}\sum_{\beta=1}^{3}\left(\alpha_{\alpha\alpha}\alpha_{\beta\beta} + 7\alpha_{\alpha\beta}\alpha_{\alpha\beta}\right) \tag{5}$$

$$I_{ROA} = 8K\sum_{\beta=1}^{3}\sum_{\alpha=1}^{3}\left(3\alpha_{\alpha\beta}G_{\alpha\beta} - \alpha_{\alpha\alpha}G_\beta + \omega\sum_{\varepsilon=1}^{3}\sum_{\gamma=1}^{3}\varepsilon_{\alpha\beta\gamma}\alpha_{\alpha\varepsilon}A_{\beta\gamma\varepsilon}\right) \tag{6}$$

where ε is the unit anti-symmetric tensor, and the constant

$$K = \frac{1}{30}\left(\frac{\omega^2\mu_0 E_0}{4\pi R}\right)^2 \tag{7}$$

where μ_0 is the vacuum permeability, E_0 is the intensity of the electric field, and R is the distance from the molecule.

From (7), we can see that the Raman intensity is proportional to the fourth power of the excitation frequency, or to λ^{-4}, where λ is the excitation wavelength. The ROA intensity is proportional to λ^{-5} because of the additional multiplications by ω in (2) and (6). As discussed in ref. [20], modern spectroscopic detectors operate in the photon counting regime, where the number of Raman and ROA scattered photons is proportional "only" to λ^{-3} and λ^{-4}, which nevertheless still brings about a significant boost for the UV region compared to excitations in the visible range.

3 | Results and Discussion

3.1 | Dependence of the Spectra on the Excitation Wavelength

The dependence of Raman scattering on the excitation wavelength is documented for dialanine in Figure 1. Raman and ROA spectra are simulated for excitations within 215–532 nm. The pre-factor in equation (7) is ignored, and the spectra are normalized to unit Raman areas, so that they can be reasonably compared at the same scale. One can see that at the shortest wavelengths primarily the bands originated in vibrations in the vicinity of the amide group are enhanced, such as the amide I (C═O stretching, calculated at 1695 cm^{-1}), amide II (1566 cm^{-1}), and the extended amide III (<1400 cm^{-1}) modes.

For longer wavelengths, on the other hand, bands such as those connected to the methyl and NH_3^+ extremities are in terms of relative intensities stronger. They include methyl torsions and delocalized molecular deformations (<200 cm^{-1}), and CH and NH stretching (>3000 cm^{-1}). A more detailed look at the dependence shows that the enhancement is not monotonic; around the 250 nm excitation the high-frequency bands have the smallest Raman intensity, which goes up both for excitations above 270 and below 240 nm.

Spectacular is also the CID ratio [15]. In the lower part of Figure 1, we can see that some parts of the 532 nm ROA spectrum are almost invisible in the same scale if compared to the 215 nm one. This reflects the extra excitation frequency dependence from the ROA tensors (**G**, **A**) discussed above. Finally, we can see that at short wavelengths the ROA spectrum is largely monosignate, roughly copying the Raman shape, which suggest conditions close to the SES limit [19].

So what are the electronic states driving the Raman and ROA spectral changes? This can be seen in Figure 2, top, where the total dynamic density and transition electronic densities for five lowest-energy electronic transitions are generated. At the lower part of the figure, ROA and Raman spectra are plotted as obtained form the limited number of states indicated. Clearly, the first π-π* amide transition [33] does not seem to significantly contribute to the intensities, which originate primarily from the two *n*-π* amide transitions, where *n* refers to the lone electron pair at the carbonyl oxygen, and π to the conjugated electron amide system. Interestingly, adding more states does not automatically lead to an increase of Raman or ROA intensities. This is nevertheless consistent with the intensity equations (5) and (6), where individual state contributions to the polarizabilities can interfere and cancel each other. Compared to the π-π* and *n*-π* amide transitions, states number 4 and 5 contribute much less. However, one has to realize much more states contribute to the final spectral patterns, and that the convergence is rather slow [16, 37].

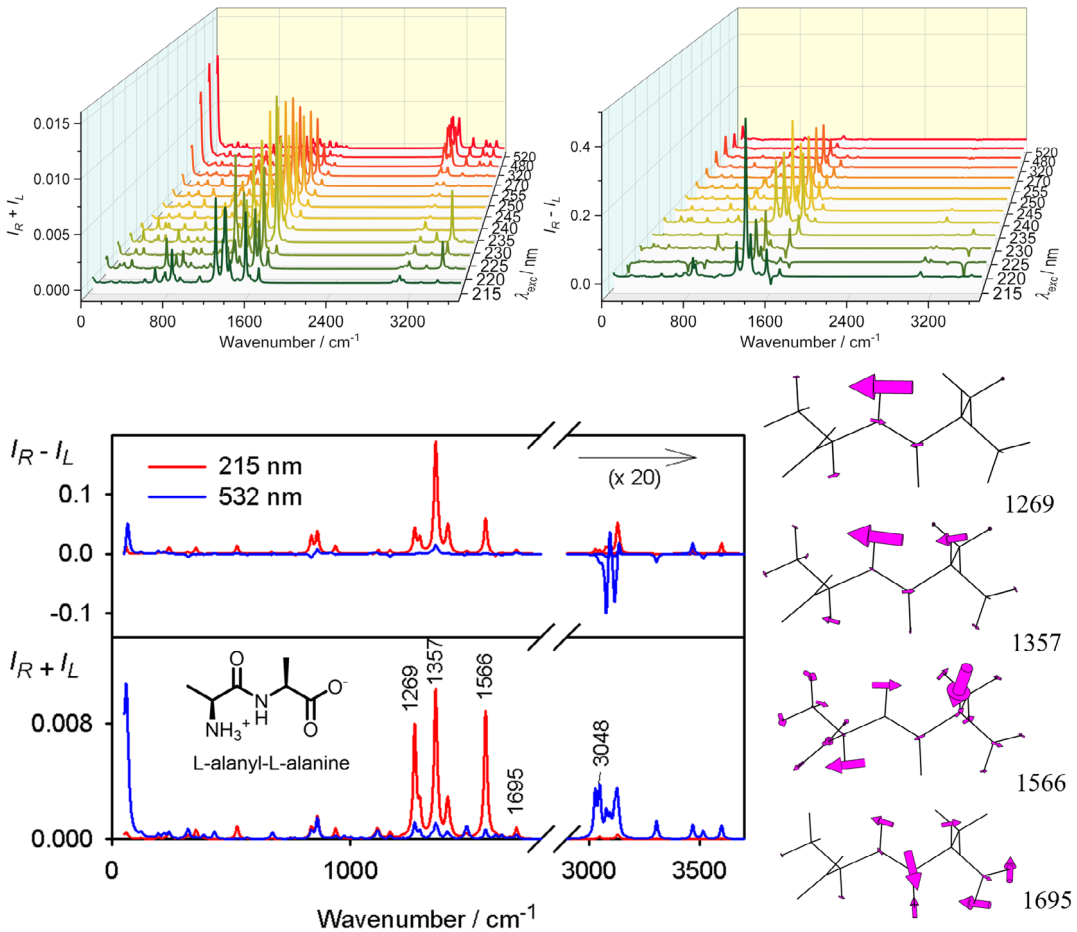

FIGURE 1 | Raman ($I_R + I_L$) and ROA ($I_R - I_L$) spectra of dialanine zwitterion for different excitation wavelengths, detailed comparison of the 215 and 532 nm results, and selected normal modes (B3PW91/6-311++G**/PCM simulation for conformer B in ref. [35], the spectra are normalized to unit Raman areas).

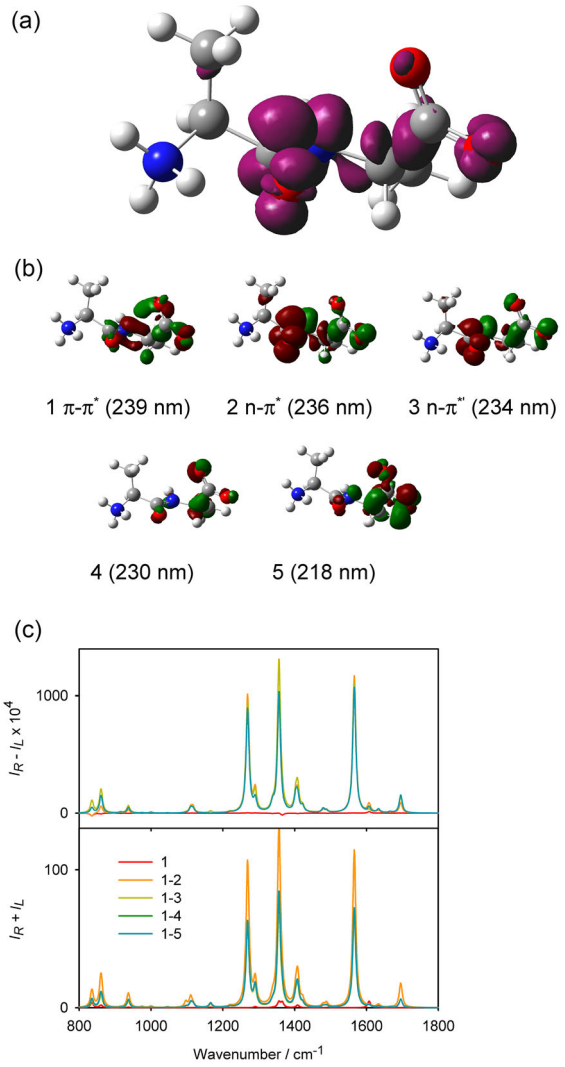

FIGURE 2 | (a) Total dynamic charge density [36] in dialanine zwitterion for the 244 nm excitation, (b) transition densities for five lowest-energy excited electronic states, and (c) ROA and Raman spectra generated from them, using the range indicated. A B3LYP/6-311++G**/PCM simulation. The colors are chosen arbitrarily, magenta for the total density, red and green for positive and negative transition densities.

3.2 | Importance of the Proper Modeling of the Aqueous Environment

Clearly, the electronic states determine the shapes of the UV ROA and Raman spectra, and they need to be accurately modeled in the simulations. This requires that also the solvent, significantly contributing to the molecular electronic properties, is described realistically. For dialanine ECD and absorption spectra, the common polarizable continuum model (PCM) reasonably well describes the overall trends, but it predicts the absorption threshold too high (Figure 3). The PCM absorption maximum around 235 nm and associated negative ECD are unseen experimentally. The combined model where water molecules of the first hydration sphere are included explicitly in the calculations and PCM is used to describe only the more distant one gives much more realistic spectral shapes. For example, the lowest-energy π-π* transition is predicted below 220 nm, and the broader ECD negative shape within ~190–220 nm reasonably well approaches the experiment. The negative ECD signal is consistent with the SES approximation which for this case predicts predominantly positive ROA [2]. From non-measurable ECD at 244 nm we can also deduce that the ECD-Raman effect [8] will be negligible in the UV ROA experiments presented below.

3.3 | Ultraviolet versus Visible Excitation Raman Scattering

The cluster averaging also gives a very good representation of the experimental Raman and ROA intensities, including differences between the 244 and 532 nm excitations. For dialanine, the data are similar to the bare PCM results (Figures 1 and 2), with more realistic bandshapes, frequencies, and intensities (Figure 4, top). For UV ROA, calculated CID appear slightly larger than the experimental one, although the latter may be affected by experimental noise. The 532 nm spectrum was analyzed in detail elsewhere [35].

The UV ROA and Raman spectra of cyclic Ala–Ala (Figure 4, bottom) are much simpler than for the linear analogue, which reflects molecular symmetry and the *cis*-amide arrangement [39]. The experimental UV ROA spectrum is dominated by a broad positive 1484 cm^{-1} amide II band, for which the theory suggests that it is composed of two positive ones. Also the calculated negative band at 1470 cm^{-1} is consistent with the overall experimental shape, albeit the experimental negative signal at 1440 cm^{-1} is weaker. The second highest UV Raman band at 1329/1319 (calculated/exp.) cm^{-1} is accompanied by a smaller positively biased ROA couplet, which is again reproduced by the computations. Similarly as for (linear) dialanine, at 532 nm excitation, ROA spectrum acquires much more features and becomes more balanced, i.e., bisignate. Since no frequency scaling was applied in the computations, for both compounds one should acknowledge systematic overestimation of the calculated frequencies. This is most visible for the highest wavenumber bands. Nevertheless, this is common in such computations, explicable by neglecting some solvation and anharmonic effects, and does not prevent unambiguous assignment of most Raman and ROA bands.

3.4 | Ala_4 Tetrapeptide Spectra and Their Conformational Dependence

Finally, for Ala_4, the results are consistent with the trends observed for the smaller molecules (Figure 5). For the 532 nm excitation, the experimental and simulated spectra are very similar to those reported in a previous work [40]. Experimental UV ROA spectrum seems to be more structured and bisignate compared to the linear and cyclic dipeptides, although with a higher noise to signal ratio is higher (the experiment had to be done at a lower 0.04 M concentration and required over 100 h of accumulation time). Similarly as for c-Ala-Ala, the bisignate character may reflect multiple amide groups and thus multiple pre-resonating electronic states contributing to the spectra.

In the simulation, the excitation wavelength (264 nm) was slightly offset from 244 nm, to avoid accidental strong resonances and to limit the number of the clusters that needed to be taken into the averaging. The computed spectra well mimic at least the most significant changes between the 532 and 244 nm experiments,

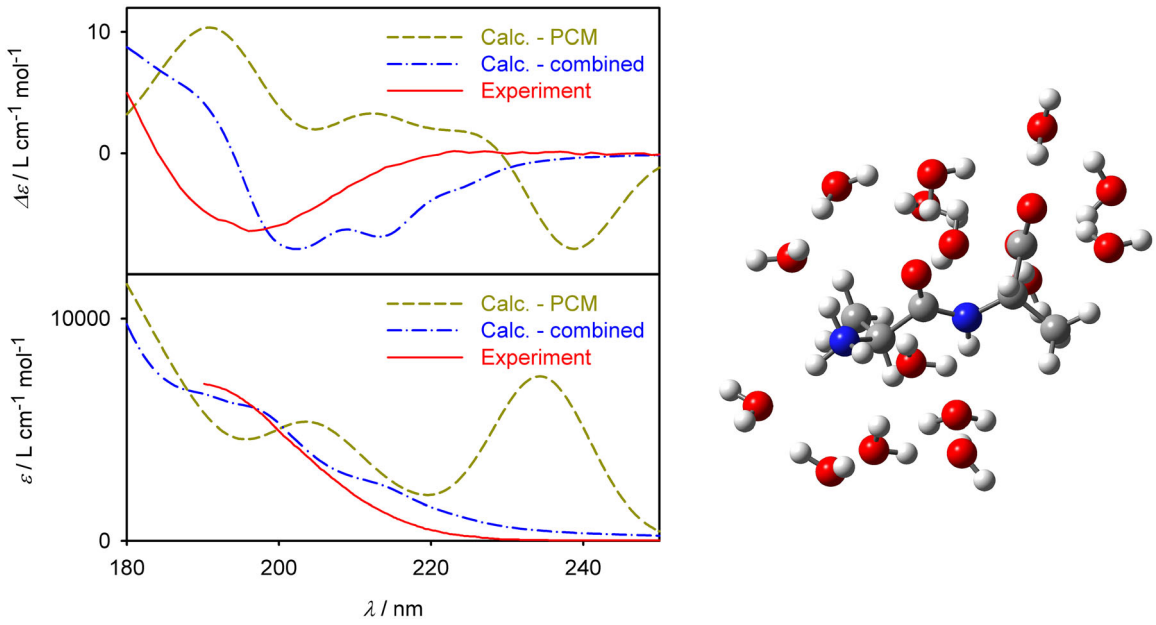

FIGURE 3 | ECD ($\Delta\varepsilon$) and absorption (ε) spectra of dialanine zwitterion, B3PW91/6-311++G** calculations with implicit (PCM) and combined (PCM and explicit waters) solvent model, and experiment from ref. [38]. Example of the clusters used in the combined modeling is given on the right.

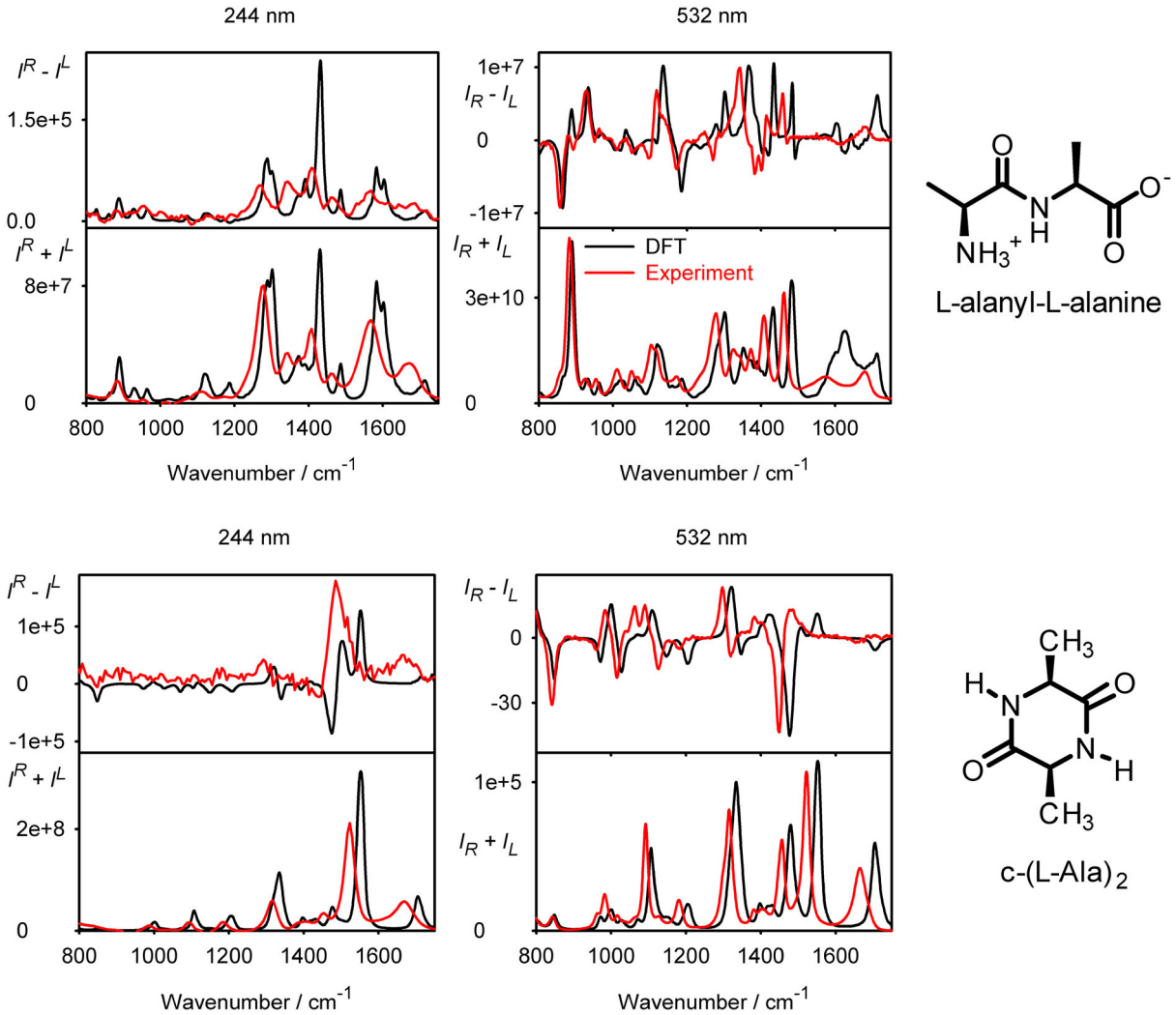

FIGURE 4 | Calculated and experimental ROA and Raman spectra of the dialanine zwitterion and c-Ala–Ala, for 244 nm (left) and 532 nm (right) excitations. The calculated spectra (B3LYP/6-311++G**/PCM, obtained as ~ 200 cluster averages) are normalized so that Raman areas in the experiment and calculation are the same (one scaling factor is used for calculated Raman and ROA).

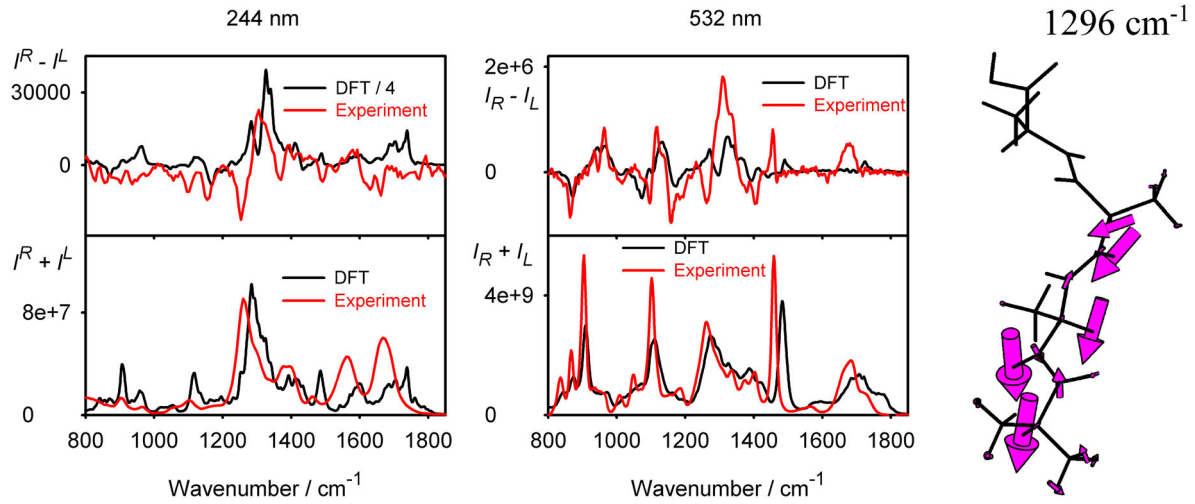

FIGURE 5 | Calculated and experimental ROA and Raman spectra of Ala_4, for the 244 nm (calculated at 264 nm) and 532 nm excitations. Calculated spectra (PPII conformation, B3LYP/6-311++G**/PCM 20 cluster average) are normalized to Raman areas, 244 nm ROA intensities were divided by four for easier comparison. On the right, example of normal mode motion contributing to the largest UV Raman band, water molecules are not shown.

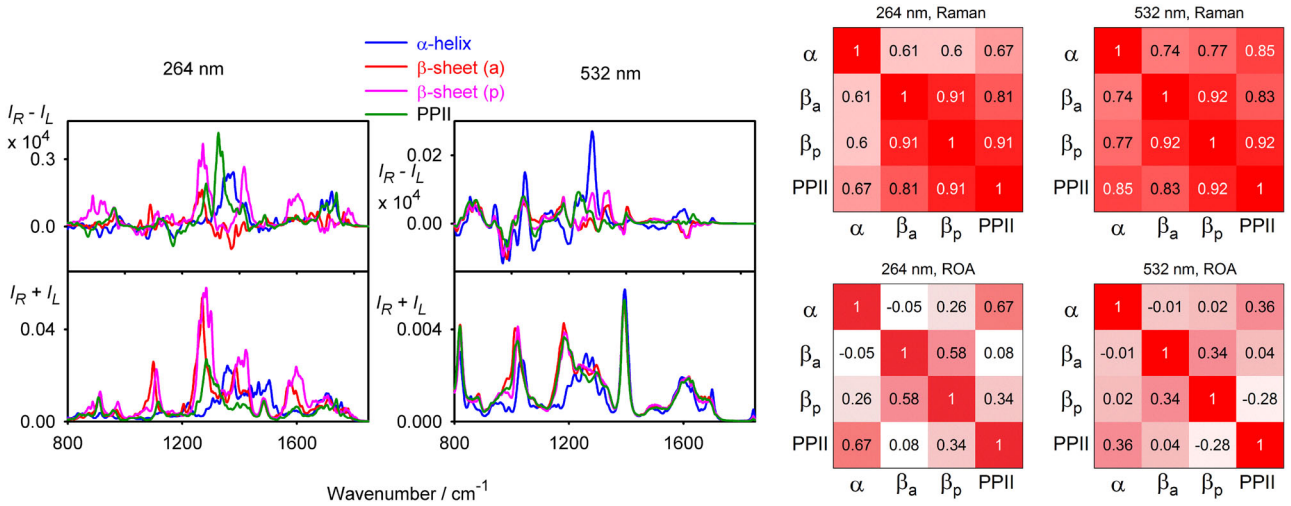

FIGURE 6 | (Left) ROA and Raman spectra of four canonical Ala_4 peptide secondary structures, simulated for the 264 and 532 nm excitations, and (right) similarity indices defined as $S_{ij} = \int S_i S_j dv / \sqrt{\int S_i^2 dv \int S_j^2 dv}$, the integrations ran within 800–1900 cm^{-1}. The B3LYP/6-311++G**/CPCM level was used, with about 20 Ala_4-water clusters averaged for each conformation.

such as the relatively huge UV Raman signal at 1262 cm^{-1} (experimentally) /1278 cm^{-1} (calculated). This is rather unexpected, given the more even band intensities in this region for dialanine, and can be partially explained by a combination of resonance effects, delocalization and vibrational mode coupling along the peptide chain, such as in the normal mode displayed in Figure 5, right. For UV ROA, computed intensities are about four times higher than the observed ones, which can be most probably attributed to a larger flexibility of the tetrapeptide than allowed in the MD PPII restrained dynamics [40].

Having in mind potential applications for protein folding studies, one may wonder if UV spectra can better discriminate peptide secondary structures than those excited in the visible range. This is yet to be seen experimentally; nevertheless, the calculated Raman and ROA spectra seem to provide useful guidance. For α-helical, antiparallel, and parallel β-sheet, and PPII conformations of Ala_4 they are compared in Figure 6, left. In Raman, only α-helix is significantly different from the other forms at 532 nm, while for the 264 excitation PPII can be clearly distinguished from the β-sheets as well. For UV ROA, the differences are even more pronounced, and the parallel and anti-parallel β-sheets give quite distinct curves.

An alternative comparison is provided by the integral similarities shown in Figure 6, right, confirming that not only the differences between α-helix and the other forms are bigger, but that also other secondary structures can be slightly better resolved in UV. Nevertheless, not always are the UV similarity indices more sensitive to the structure; for example, parallel and antiparallel β-sheet UV ROA spectra are more similar ($s = 0.58$) than for the 532 nm excitation ($s = 0.34$). Overall, however, the added structural sensitivity is clearly another benefit of UV ROA, in addition to higher sensitivity and lower fluorescence.

The spectral shapes compared in the figure suggest that the $^{\alpha}$CH bending region around 1300 cm^{-1}, so important for visible ROA [41], gives the biggest differences also in UV; in addition, the spectra differ more in other wavenumber regions.

In summary, the results suggest that UV ROA spectroscopy will be useful for peptide and protein studies and that available computational tools provide a good theoretical basis for the observations. Compared to the theory, experimental protocols appear more problematic, as even the small molecules studied here were quickly decomposing in the UV laser beam, which resulted in the need of a spinning sample cell, low laser powers, low concentrations, and consequently, long accumulation time and noisy spectra.

4 | Conclusion

For the first time, we obtained reliable ROA spectra in the deep UV region, could verify the results by measurement of both enantiomers, and analyze them on the basis of accurate density functional computations. The results showed that the pre-resonance theoretical approach is adequate for the 244 nm experiments. Realistic approximation of the aqueous environment, including explicit water molecules, appeared critical for accurate simulations. Both the experimental and computed data confirm the theoretical premises: (1) the UV light brings about an increase of Raman and ROA intensities, (2) the ROA/Raman intensity ratio increases as well, and (3) the electronic transitions at the amide chromophore are driving the 532 nm → 244 nm Raman spectral changes. The contribution of the n-π* transition to Raman and ROA intensities was found larger than that of the π-π* transition. The computational experiment with Ala_4 suggests that UV ROA spectra are even more sensitive to peptide and protein secondary structures than the classical Raman spectroscopy with visible light, although this result needs to be experimentally verified in the future. With the established experimental background and robust simulation apparatus, the UV Raman and ROA spectroscopy thus appear ripe for analytical applications, such as for peptide and protein structural studies.

5 | Experimental Section

5.1 | Raman and ROA Spectra Measurement

The spectra were collected using Biotools 532 nm and custom-made [20] 244 nm ROA spectrometers in backscattering SCP and ICP modulation schemes, respectively. To limit degradation, samples for the 244 nm measurements were held in a spinning cylindrical quartz cell (Starna, spinning speed 500–1000 rpm, diameter of 20 mm, and path length of 10 mm). The spinning appeared convenient also for dust particles and precipitates being pushed by centrifugal force from the laser beam, unlike for peristaltic a pump sometimes also used for photosensitive samples [42, 43]. Both the L and D enantiomers were used, to verify the signal, detailed experimental conditions are summarized in Table S1 in the Supporting Information. Commercial chemicals (Sigma–Aldrich) were used and dissolved in distilled water (dialanine, cyclo-dialanine) and HCl solution (tetraalanine, pH 1). Idealized L-enantiomer spectra ["(L + D)/2" for Raman and "(L-D)/2" for ROA] are presented in the main text, for Raman a minor baseline correction was done for better comparison with the theory. Although in the preresonance regime, the SCP and ICP intensities are the same, and the scattered and incident polarizations are indicated in the graphs as lower and upper indices, respectively (I_R, I^R, etc.), to follow the convention.

5.2 | Spectral Simulations

For a single molecule model of dialanine, initial geometry was taken from ref. [35], conformation B, optimized by energy minimization with torsion angles fixed to (ϕ, ψ) = (−73°, 152°), and UV absorption and ECD intensities were computed using the Gaussian program [34] at the B3PW91/6-311++G**/PCM level. Smooth spectra were obtained by a convolution with Gaussian functions. For selected $0 \rightarrow e$ electronic transitions, transition densities were generated as $\rho = \sum_{\{ab\}} c^e_{ab} \phi_a \phi_b$, where c^e_{ab} are the configuration coefficients obtained by the time-dependent DFT computation, and ϕ_a are molecular orbitals. The same level and software were used for the Raman and ROA intensities calculated at several excitation wavelengths and the harmonic approximation. Smooth spectra were generated as $S(\omega) = \sum_i I_i \left[1 - \exp\left(-\frac{\omega_i}{kT}\right)\right]^{-1} \left[4\left(\frac{\omega - \omega_i}{\Delta}\right)^2 + 1\right]^{-1}$ where I_i are the line intensities, ωi are vibrational frequencies, k is the Boltzmann constant, T is the temperature (300 K), and Δ = 15 cm^{-1}. Alternatively, using our scripts [16], the polarizabilities were calculated directly using the sum over states expressions (1–3), from a few electronic excited states (energies and transition moments) calculated by Gaussian within the time-dependent DFT. This allowed us to estimate approximate contributions of individual electronic states to Raman and ROA intensities.

To better describe the aqueous environment, molecular dynamics (MD) was performed within the Amber software [44]. For dialanine, MD trajectories from ref. [35] were used. The c-Ala-Ala and $(Ala)_4$ peptides were put in a $(40\ Å)^3$ cubical box otherwise filled with water, and after equilibration stages production dynamics ran for 1 ns, using an *nVT* ensemble, temperature of 300 K (stabilized by the Langevin thermostat), and 1 fs integration time. For c-Ala-Ala, free dynamics was performed, while for $(Ala)_4$ backbone torsion angles (φ, ψ) were constrained to mimic α-helical, parallel, and antiparallel β-sheet and polyproline II (PPII) standard protein conformations [45]. Note that polyproline II is a good model of disordered peptides and proteins [46] as well as for the Ala_4 peptide [40]. Cluster averaging included 75 snapshots of each of the A, B, C, and D dialanine conformer [35], 200 snapshots of c-Ala–Ala, and 100 snapshots of each $(Ala)_4$ standard conformation. The snapshots were separated at least by 1 ps (1000 MD steps). For computation of the absorption and ECD dialanine spectra, 10 snapshots were averaged for each conformer. Clusters of the peptide and water molecules were created by keeping only waters closer than 3.6 Å to the peptide. These were then partially optimized using the vibrational normal mode coordinates at the B3LYP/6-311++G**/PCM level [47]; modes with frequencies smaller than 300 cm^{-1} were fixed. Control computations showed that the B3LYP and B3PW91 functionals gave nearly same results; the latter one was used for Ala-Al for consistency with ref [35]. At the same approximation level, electronic and vibrational spectra were calculated using the Gaussian program.

Acknowledgments

The work was supported by the Grant Agency of the Czech Republic (25-15726S).

Open access publishing facilitated by Ustav organicke chemie a biochemie Akademie ved Ceske republiky, as part of the Wiley - CzechELib agreement.

Funding

This study was supported by Grantová Agentura České Republiky (25-15726S).

Conflicts of Interest

The authors declare no conflicts of interest.

Data Availability Statement

The data that support the findings of this study are available in the supplementary material of this article.

References

1. S. A. Asher, M. Chalmers, and P. R. Griffiths, *In Handbook of Vibrational Spectroscopy*. eds.: J. M. Chalmers, P. R. Griffiths, (John Wiley & Sons Ltd., 2002).

2. L. Nafie, *Vibrational Optical Activity: Principles and Applications*. (Wiley, 2011).

3. T. Wu, J. Kapitán, and P. Bouř, "Resolving Resonant Electronic States in Chiral Metal Complexes by Raman Optical Activity Spectroscopy," *The Journal of Physical Chemistry Letters* 13 (2022): 3873.

4. Z. Osifová, T. Kalvoda, J. Galgonek, et al., "What Are the Minimal Folding Seeds in Proteins? Experimental and Theoretical Assessment of Secondary Structure Propensities of Small Peptide Fragments," *Chemical Science* 15 (2024): 594.

5. M. Dudek, G. Zajac, A. Kaczor, and M. Baranska, "Aggregation-Induced Resonance Raman Optical Activity (AIRROA) and Time-Dependent Helicity Switching of Astaxanthin Supramolecular Assemblies," *The Journal of Physical Chemistry. B* 120 (2016): 7807.

6. D. Kurouski, R. K. Dukor, X. Lu, L. A. Nafie, and I. K. Lednev, "Spontaneous Inter-Conversion of Insulin Fibril Chirality," *Chemical Communications* 48 (2012): 2837.

7. M. Pazderková, T. Pazderka, M. Shanmugasundaram, R. K. Dukor, I. K. Lednev, and L. A. Nafie, "Origin of Enhanced VCD in Amyloid Fibril Spectra: Effect of Deuteriation and pH," *Chirality* 29 (2017): 469.

8. T. Wu, G. Li, J. Kapitán, J. Kessler, Y. Xu, and P. Bouř, "Two Spectroscopies in One: Interference of Circular Dichroism and Raman Optical Activity," *Angewandte Chemie International Edition* 59 (2020): 21895.

9. G. Li, M. Alshalalfeh, W. Yang, J. R. Cheeseman, P. Bouř, and Y. Xu, "Can One Measure Resonance Raman Optical Activity?," *Angewandte Chemie International Edition* 60 (2021): 22004.

10. J. Šebestík, J. Kapitán, O. Pačes, and P. Bouř, "Diamagnetic Raman Optical Activity of Chlorine, Bromine, and Iodine Gases," *Angewandte Chemie International Edition* 55 (2016): 3504.

11. G. Zajac, A. Kaczor, A. P. Zazo, J. Mlynarski, M. Dudek, and M. Baranska, "Aggregation-Induced Resonance Raman Optical Activity (AIRROA): A New Mechanism for Chirality Enhancement," *The Journal of Physical Chemistry. B* 120 (2016): 4028.

12. Q. Yang, V. Andrushchenko, J. Hudecová, et al., "Black-Box Simulations of Anharmonic Vibrational Chiroptical Spectra: Problems with Property Third Derivatives and the Solvent," *Journal of Chemical Theory and Computation* 21 (2025): 10489–10502.

13. M. Born and R. Oppenheimer, "Zur Quantentheorie der Molekeln," *Annalen der Physik* 389 (1927): 457.

14. G. Placzek, *Handbuch der Radiologie*. ed: E. Marx, (Akademische Verlagsgesellschaft, 1934), 205.

15. L. D. Barron, *Molecular Light Scattering and Optical Activity*. (Cambridge University Press, 2004).

16. J. Šebestík and P. Bouř, "Quantum Chemical Computations of Raman Intensities: An Ambiguity of the Placzek Approximation," *Physical Review. A, Atomic, Molecular, and Optical Physics* 111 (2025): 062804.

17. Q. Yang, J. Bloino, H. Šestáková, et al., "Combination of Resonance and Non-Resonance Chiral Raman Scattering in a Cobalt(III) Complex," *Angewandte Chemie International Edition* 62 (2023): e202312521.

18. J. R. Cheeseman and P. Bouř, "Adaptive Excitation Frequencies in Simulations of Resonance Raman Spectra," *The Journal of Chemical Physics* 163 (2025): 034118.

19. L. A. Nafie, "Theory of Resonance Raman Optical Activity: The Single Electronic State Limit," *Chemical Physics* 205 (1996): 309.

20. J. Kapitán, L. D. Barron, and L. Hecht, "A Novel Raman Optical Activity Instrument Operating in the Deep Ultraviolet Spectral Region," *Journal of Raman Spectroscopy : Jrs* 46 (2015): 392.

21. J. Kapitán, V. Baumruk, R. Pohl V. Kopecký Jr., and P. Bouř, "Proline Zwitterion Dynamics in Solution, Glass and Crystalline State," *Journal of the American Chemical Society* 128 (2006): 13451.

22. W. Hug, J. M. Chalmers, and P. R. Griffiths, *In Handbook of Vib. Spectrosc*. eds.: J. M. Chalmers, P. R. Griffiths, (John Wiley, 2002).

23. M. Unno, T. Kikukawa, M. Kumauchi, and N. Kamo, "Exploring the Active Site Structure of a Photoreceptor Protein by Raman Optical Activity," *The Journal of Physical Chemistry. B* 117 (2013): 1321.

24. L. A. Nafie, B. E. Brinson, X. Cao, et al., "Near-Infrared Excited Raman Optical Activity," *Applied Spectroscopy* 61 (2007): 1103.

25. P. L. Polavarapu, "Fourier Transform Raman Optical Activity," *Chemical Physics Letters* 148 (1988): 21.

26. J. R. Cheeseman and M. J. Frisch, "Basis Set Dependence of Vibrational Raman and Raman Optical Activity Intensities," *Journal of Chemical Theory and Computation* 7 (2011): 3323.

27. K. Ruud, T. Helgaker, and P. Bouř, "Gauge-Origin Independent Density-Functional Theory Calculations of Vibrational Raman Optical Activity," *The Journal of Physical Chemistry. A* 106 (2002): 7448.

28. P. Bouř and T. A. Keiderling, "Ab Initio Simulation of the Vibrational Circular Dichroism of Coupled Peptides," *Journal of the American Chemical Society* 115 (1993): 9602.

29. T. A. Keiderling, "Structure of Condensed Phase Peptides: Insights from Vibrational Circular Dichroism and Raman Optical Activity Techniques," *Chemical Reviews* 120 (2020): 3381.

30. L. D. Barron, L. Hecht, I. H. McColl, and E. W. Blanch, "Raman Optical Activity Comes of Age," *Molecular Physics* 102 (2006): 731.

31. L. Hecht and L. A. Nafie, "Theory of Natural Raman Optical Activity," *Molecular Physics* 72 (2006): 441.

32. A. Baiardi, J. Bloino, and V. Barone, "Time-Dependent Formulation of Resonance Raman Optical Activity Spectroscopy," *Journal of Chemical Theory and Computation* 14 (2018): 6370.

33. N. Berova, K. Nakanishi, and R. W. Woody, (Wiley-VCH, 2000).

34. M. J. Frisch, G. W. Trucks, H. B. Schlegel, et al., *Gaussian, Inc*. (Wallingford, CT, 2016).

35. J. Jungwirth, J. Šebestík, M. Šafařík, J. Kapitán, and P. Bouř, "Quantitative Determination of Ala-Ala Conformer Ratios in Solution

by Decomposition of Raman Optical Activity Spectra," *The Journal of Physical Chemistry. B* 121 (2017): 8956.

36. O. Škrna, J. Kessler, Z. Liu, S. Che, and P. Bouř, "Reproduction of Chiral Anisotropy in Surface-Enhanced Raman Scattering on Gold Nanowires by Computational Modeling," *The Journal of Physical Chemistry C* 128 (2024): 12649.

37. J. P. Coe and M. J. Paterson, "Approaching Exact Hyperpolarizabilities via Sum-over-States Monte Carlo Configuration Interaction," *The Journal of Chemical Physics* 141 (2014): 124118.

38. J. Šebek, B. Gyurscik, J. Šebestík, Z. Kejík, L. Bernárová, and P. Bouř, "Interpretation of Synchrotron Radiation Circular Dichroism Spectra of Anionic, Cationic, and Zwitterionic Dialanine Forms," *The Journal of Physical Chemistry. A* 111 (2007): 2750.

39. T. Miyazawa, "Normal Vibrations of Monosubstituted Amides in the Cis Configuration and Infrared Spectra of Diketopiperazine," *Journal of Molecular Spectroscopy* 4 (1960): 155.

40. M. Furuta, T. Fujisawa, H. Urago, et al., "Raman Optical Activity of Tetra-Alanine in the Poly(l-Proline) II Type Peptide Conformation," *Physical Chemistry Chemical Physics : Pccp* 19 (2017): 2078.

41. J. Kessler, J. Kapitán, and P. Bouř, "First-Principles Predictions of Vibrational Raman Optical Activity of Globular Proteins," *The Journal of Physical Chemistry Letters* 6 (2015): 3314.

42. L. D. Barron, J. Vrbancich, and R. S. Watts, "Magnetic Resonance-Raman Optical Activity of IrBr2−6," *Chemical Physics Letters* 89 (1982): 71.

43. L. D. Barron, J. Vrbancich, *Advances in Infrared and Raman Spectroscopy*. eds.: R. J. H. Clark, R. E. Hester, (Wiley, 1985), 215.

44. D. A. Case, I. T. E. Cheatham, T. Darden, et al., "The Amber Biomolecular Simulation Programs," *Journal of Computational Chemistry* 26 (2005): 1668.

45. T. E. Creighton, *Proteins: Structures and Molecular Properties*. 2nd, (W. H. Freeman and Co, 1993).

46. R. K. Dukor and T. A. Keiderling, "Reassessment of the Random Coil Conformation: Vibrational CD Study of Proline Oligopeptides and Related Polypeptides," *Biopolymers* 31 (1991): 1747.

47. P. Bouř and T. A. Keiderling, "Partial Optimization of Molecular Geometry in Normal Coordinates and use as a Tool for Simulation of Vibrational Spectra," *The Journal of Chemical Physics* 117 (2002): 4126.

Supporting Information

Additional supporting information can be found online in the Supporting Information section. Experimental conditions and raw experimental spectra.